

# Measurement of linewidths and permanent electric dipole moment change of the Ce $4f-5d$ transition in $Y_2SiO_5$ for qubit readout scheme in rare-earth ion based quantum computing

Ying Yan,<sup>\*</sup> Jenny Karlsson, Lars Rippe, Andreas Walther, Diana Serrano, David Lindgren, Mats-erik Pistol, and Stefan Kröll  
*Department of Physics, Lund University, P.O. Box 118, SE-22100 Lund, Sweden*

Philippe Goldner

*Chimie ParisTech, Laboratoire de Chimie de la Matière Condensée de Paris, CNRS-UMR 7574, UPMC Université Paris 06,  
 11 rue Pierre et Marie Curie 75005 Paris, France*

Lihe Zheng and Jun Xu

*Key Laboratory of Transparent and Opto-Functional Inorganic Materials, Shanghai Institute of Ceramics, Chinese Academy of Sciences,  
 Shanghai 201800, China*

(Received 18 February 2013; revised manuscript received 2 May 2013; published 30 May 2013)

In this work the inhomogeneous (zero-phonon line) and homogeneous linewidths and the permanent electric dipole moment change (averaged value of all dipole orientations) for the Ce  $4f-5d$  transition in  $Y_2SiO_5$  were measured in order to investigate the possibility for using Ce as a sensor to detect the hyperfine state of a spatially close-lying Pr or Eu ion. The experiments were carried out on Ce doped or Ce-Pr co-doped single  $Y_2SiO_5$  crystals. The homogeneous linewidth is essentially limited by the excited state lifetime. Based on the linewidth measurements, the oscillator strength, absorption cross section, and saturation intensity were calculated to be about  $6.2(\pm 1.7) \times 10^{-7}$ ,  $4.5(\pm 1.3) \times 10^{-19} \text{ m}^2$ , and  $1.4(\pm 0.4) \times 10^7 \text{ W/m}^2$ , respectively. The difference in permanent dipole moment,  $\Delta\mu_{Ce}$ , between the ground and excited states of the Ce ion was measured as  $9.6(\pm 5.3) \times 10^{-30} \text{ C m}$ . These measurements indicate that Ce is a promising readout ion to probe a single-ion qubit state for the quantum computing scheme using rare-earth ions.

DOI: [10.1103/PhysRevB.87.184205](https://doi.org/10.1103/PhysRevB.87.184205)

PACS number(s): 33.70.Jg, 78.47.jh, 42.50.Md

## I. INTRODUCTION

The quantum computing research field has attracted extensive interest for its potential to give a tremendous boost in computational ability for certain types of problems. Many physical systems have been investigated as test beds for quantum computing:<sup>1</sup> trapped ions,<sup>2</sup> nuclei in molecules,<sup>3</sup> Josephson junctions in superconductors,<sup>4</sup> nitrogen vacancy centers in diamond,<sup>5</sup> rare-earth ions in inorganic crystals,<sup>6</sup> etc. Regardless of the physical system, one of the necessary criteria for a quantum computing scheme is that it should be scalable. In this paper rare-earth ions based quantum computing (REIQC) is under concern, and the results in this paper are a part of the work to develop an ability to read out the hyperfine state of single ions in a rare-earth crystal in order to obtain a scalable system. In REIQC qubit-qubit interaction and arbitrary single qubit rotations have been carried out.<sup>7,8</sup> In these experiments each qubit, where the qubit states ( $|0\rangle$  and  $|1\rangle$ ) are two ground-state hyperfine levels of the ion, was represented by an ensemble of ions and addressed via their optical transition frequencies.<sup>8</sup> The optical transition lines of rare-earth ions in a crystal are inhomogeneously broadened as a result of the random substitutions of the rare-earth ions (qubit ions) in the solid matrix, which causes slight crystal-field variations for the sites of the individual ions. The ratio between the inhomogeneous and homogeneous broadening in these systems can be larger than  $10^6$ . Thus a very large number of subensembles of ions can be singled out in frequency space within the inhomogeneous line. Each subensemble can then act as a frequency-selectively addressed qubit although they consist of many ions randomly distributed in space. The

conditional gate operations in these systems can be realized via the permanent electric dipole-dipole interaction between the strong-interacting ions in each qubit (see Figs. 3 and 11 in Ref. 9 for details). The strength of the dipole-dipole interaction between two ions depends on the spatial distance between them,  $r$ , as  $1/r^3$ . Because of this spatially dependent coupling and the random spatial distribution of the ions in each qubit, the average probability  $P$  of an ion in one qubit being sufficiently close to an ion in another qubit to control its state is often  $\ll 1$  for reasonable dopant concentrations. This means that the number of active ions in one ensemble qubit that interact strongly with one ion in each of the rest of the  $n - 1$  qubits scales as  $P^{n-1}$ . In order to improve this poor scalability, Wesenberg *et al.* proposed several schemes.<sup>10</sup> One approach is to discard the ensemble qubits and instead let each single ion represent a qubit. With sufficient dopant concentration, for instance 0.2% for Pr: $Y_2SiO_5$ , there is a large possibility to find sequences of ions which sit  $\sim 3 \text{ nm}$  (on average) away from each other and where each of these absorbs at a specific and unique optical frequency and represents one single qubit. With that separation the dipole-dipole interaction between the qubits are strong enough for carrying out gate operations.<sup>11</sup>

However, in this single instance quantum computing approach a technique to read out the quantum state of a single-ion qubit needs to be developed. The straightforward typical fluorescence measurement for detecting a single molecule does not work because, first, the transitions of the qubit ion (in Ref. 8 this has been a Pr ion), which can discriminate the qubit states, have excited state lifetimes of more than  $10 \mu\text{s}$ , which provides too low an emission rate for a high signal-to-noise detection; second, and more importantly, the qubit ion candidates have

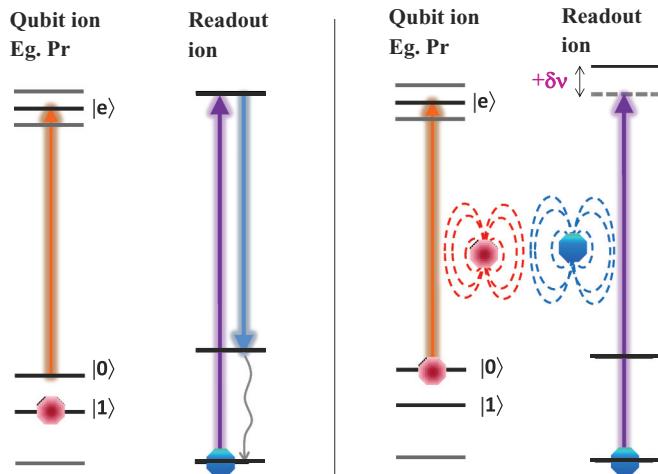


FIG. 1. (Color online) Permanent dipole-dipole interaction between a qubit ion and a readout ion that sits spatially close to this qubit ion. Two lasers interact with the ions, one for the qubit ion and one for the readout ion. The qubit laser sends out a pulse with pulse area of  $\pi$  on the  $|0\rangle \rightarrow |e\rangle$  transition and following this pulse the readout laser is turned on and continuously excites the readout ion. If the Pr ion is in state  $|1\rangle$  (left panel), the qubit laser is not on resonance with the Pr ion transition so it will not pump the Pr ion to state  $|e\rangle$ . There is no interaction between the qubit and readout ion in this case. The readout ion continuously sends out fluorescence photons (ON). On the other hand, if the Pr ion is initially in state  $|0\rangle$  (right panel), it will be excited by the qubit laser pulse. Since the permanent dipole moment of the Pr ion in state  $|e\rangle$  is different from that in state  $|0\rangle$ , the change of this local electric field induces a frequency shift ( $\delta\nu$ ) of the nearby readout ion transition line. If the shift is larger than the homogeneous linewidth, the readout ion will be out of resonance with the readout laser and never excited so there is no fluorescence (OFF).

more than one ground-state hyperfine level to which they can decay, thus there is no transition that can be cycled until the number of emitted photons is sufficiently large to provide state selective information. A single-ion readout idea was proposed in Ref. 10 to accomplish single-qubit ion detection: an additional ion (hereafter called a readout ion) can be co-doped into the crystal, with such low concentration that there is only one readout ion fluorescing within the laser focal volume. This ion serves as a sensor for reading out the state of nearby qubit ions through the interaction between the qubit and readout ion, illustrated in Fig. 1. As a result the fluorescence signal from the single readout ion, either ON or OFF, depends on whether the single qubit ion is in state  $|1\rangle$  or in  $|0\rangle$ .<sup>12</sup> For the other qubits, which are not directly coupled to the readout ion, their state can be transferred consecutively to its nearby ions through conditional gate operations until the qubit, which is directly coupled to the readout ion, is reached. Then its state can be read out in the way described above (see Sec. III B in Ref. 10 for details).

The readout scheme above requires that the readout ion has the following characteristics: (i) short excited-state lifetime in order to obtain a large contrast in photon emission number per unit time between when the qubit is in the ground state and when it is in the excited state; (ii) narrow homogeneous absorption linewidth such that the permanent dipole-dipole

interaction with a nearby qubit shifts the readout ion resonance frequency by several homogeneous linewidths; (iii) large dipole moment change between ground and excited state (again such that the shift due to the permanent dipole-dipole interaction is sufficiently large); (iv) no fluorescence quenching mechanisms, e.g., a long-lived trapping state or energy transfer from the readout ion to the qubit ion. In this work  $\text{Ce}^{3+}$  (doped in an  $\text{Y}_2\text{SiO}_5$  crystal) is considered as a readout ion.<sup>13</sup> Ce ions in  $\text{Y}_2\text{SiO}_5$  have a short excited-state lifetime of about 40 ns,<sup>14–16</sup> to be compared with an excited-state lifetime of possible qubit ions as, e.g., Pr and Eu which are about 0.2 and 2 ms, respectively. The  $4f-5d$  zero-phonon absorption line of  $\text{Ce}^{3+}$  doped in  $\text{Y}_2\text{SiO}_5$  lies around 370.83 nm, which is well separated from the qubit transition frequencies (e.g., 606 nm for Pr ions in site 1). However, other than the excited-state lifetime, the spectroscopic parameters relevant for the readout scheme are not known. In this paper, the second and third spectroscopic requirements, (ii) and (iii) above, for a readout ion were measured for Ce ions in  $\text{Y}_2\text{SiO}_5$  crystals. The inhomogeneous zero-phonon line (ZPL) measurement is described in Sec. II A, the homogeneous linewidth measurement is discussed in Sec. II B, and the measurement (based on the Ce-Pr interaction) of the Ce permanent dipole moment difference between the ground and excited state is described in Sec. II C. The work is concluded in Sec. III.

## II. DETERMINATION OF SPECTROSCOPIC PARAMETERS OF Ce IONS

We focused on the parameters that are of special interest to the single-ion readout scheme in REIQC.

### A. Zero-phonon line (ZPL) of Ce ions in an $\text{Y}_2\text{SiO}_5$ crystal

The absorption line of interest is the  $4f-5d$  transition of Ce ions as illustrated in Fig. 2(a). Since the  $5d$  levels are less shielded from the environment than the  $4f$  levels, the  $4f-5d$  transitions are often largely broadened by the external perturbations, for instance, defects in the crystal or electron-phonon coupling to the crystal lattice. The experiments were carried out at 2 K to greatly reduce the phonon broadening influence. In this and the following experiments, an external cavity diode laser in a Littrow configuration was used as an excitation source.

The inhomogeneous ZPL of  $\text{Ce}^{3+}$  was measured on a Ce: $\text{Y}_2\text{SiO}_5$  crystal with a nominal dopant concentration of 0.088 at.% relative to the yttrium ions. The result is shown in Fig. 3. Crosses are the experimental data and the solid curve is a Gaussian fit. The measured inhomogeneous linewidth is about 50 GHz (full width at half maximum of the absorption coefficient) with the line center at 370.83 nm. No significant polarization dependence was observed for the absorption. Based on the data shown in Fig. 3, the oscillator strength of the zero-phonon transition was calculated to be  $\sim 6.2(\pm 1.7) \times 10^{-7}$  using the relations shown in Refs. 17 and 18.

The ZPL shown in Fig. 3 sits on a background absorption with  $\alpha \simeq 3.6 \text{ cm}^{-1}$ , which most likely comes from the absorption by Ce ions in site 2. More information about this is provided by a fluorescence spectrum with an online excitation

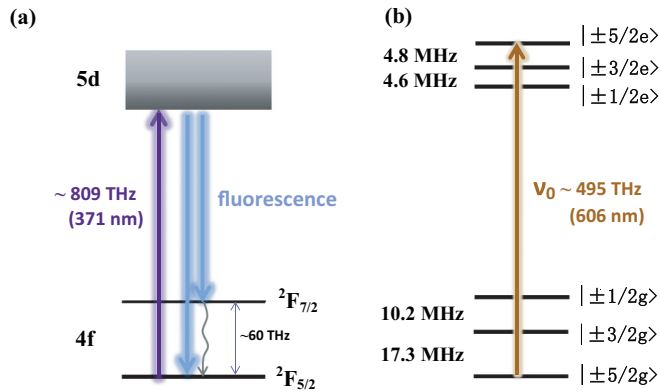


FIG. 2. (Color online) (a) Schematic level structure of  $\text{Ce}^{3+}$  in  $\text{Y}_2\text{SiO}_5$ . (b) Schematic level structure for the  ${}^3H_4 \rightarrow {}^1D_2$  transition of  $\text{Pr}^{3+}$  in  $\text{Y}_2\text{SiO}_5$ .

(at 370.83 nm) and an offline excitation (at 371.53 nm), shown as the solid and dashed curves in Fig. 4. The solid (dashed) curve matches reasonably well with the spectrum from a site 1 (site 2) excitation, shown in Refs. 19 and 14. However, the solid curve contains an extra shoulder sitting around 440 nm, the origin of which is unknown to us. In the rest of the paper, all calculations on  $\text{Ce}^{3+}$  refer to the ions in site 1, with the site 2 contribution being subtracted as a background.

### B. Homogeneous linewidth of the ZPL

The homogeneous linewidth was measured by intensity modulated saturation spectroscopy, where both the pump and probe beams were generated from the external cavity diode laser by a beam splitter (70 : 30). Both beams were focused by a 200 mm focal length lens (focal diameter  $\sim 85 \mu\text{m}$ ) onto the  $\text{Ce}:\text{Y}_2\text{SiO}_5$  crystal, which was immersed in liquid helium. The probe beam propagated at an angle of  $\sim 3^\circ$  relative to the pump beam in order to separate the two beams for the detection. Two acousto-optical modulators (AOMs) were used in series in the probe beam line. The +1 order deflected beam from the first AOM was used and followed by the -1 order deflected beam from the second AOM. In this way the probe beam frequency could be tuned within a  $\pm 50$ -MHz range relative to the pump

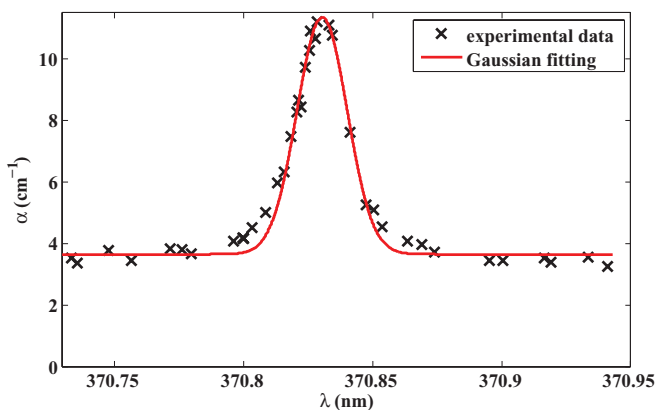


FIG. 3. (Color online) The inhomogeneous ZPL of  $\text{Ce}^{3+}$  (site 1) in an  $\text{Y}_2\text{SiO}_5$  crystal. The linewidth is about 50 GHz.  $\alpha$  is the absorption coefficient.

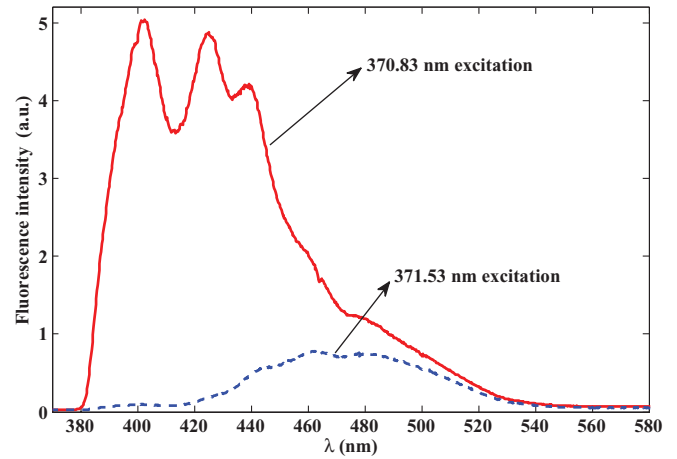


FIG. 4. (Color online) Fluorescence spectrum of  $\text{Ce}^{3+}$  in a  $\text{Ce}:\text{Y}_2\text{SiO}_5$  crystal with 370.83-nm excitation (online of site 1) (solid line) and 371.53-nm excitation (offline of site 1) (dashed line).

beam frequency by adjusting the radio frequency of the second AOM. The probe beam position movement caused by the AOM at different detuning frequencies was compensated by slightly adjusting the mirror in front of the cryostat to overlap the two beams by maximizing the probe beam transmission. The probe beam was monitored by a photodiode after the cryostat. However, it is hard to directly detect an increase of the transmitted power caused by the saturation of the pump beam, since the top-hat pump beam intensity is only of the level of 1% of the estimated saturation intensity. To improve the signal-to-noise ratio, a chopper wheel was used to modulate the intensities of the pump and probe beam with modulation frequencies of 302 and 362 Hz, respectively. Due to the nonlinear interaction, the transmitted probe beam not only has the primary frequency modulation but also has an intensity modulation at the sum (664 Hz) and difference frequency (60 Hz). The signal strength at 664 Hz was extracted from the Fourier transform of the transmitted power of the probe beam and recorded as a function of the detuning frequencies between the pump and probe beams,  $\Delta f$ .

In the experiment, the observed signal at 664 Hz was 16 times as high as the noise floor when  $\Delta f$  is zero but only 1.3% of the signal strength at 362 Hz. The measurement data are shown in Fig. 5, where the vertical axis shows the sum frequency signal normalized by the square of the input probe beam power to compensate for the change in laser power between the data points. Figure 5 reveals a spectral hole width (full width at half maximum) of about 5.8 MHz, which results from a convolution of the laser line (Lorentzian) with the homogeneous line of the transition (Lorentzian) for both the pump step and probe step.<sup>20</sup> However, only fast laser frequency fluctuations within the time scale of the excited-state lifetime ( $\sim 40$  ns) would affect the measurement. This contribution should be negligible considering that the typical linewidth of an external cavity diode laser is 300 kHz over 100  $\mu\text{s}$ . So the homogeneous linewidth we measured has an upper bound of 2.9 MHz. The 40-ns lifetime stated in the literature<sup>14–16</sup> poses a lower limit on the linewidth of  $\sim 4$  MHz. The reason for measuring a linewidth  $< 4$  MHz might be that the signal at positive detuning frequencies was not properly maximized

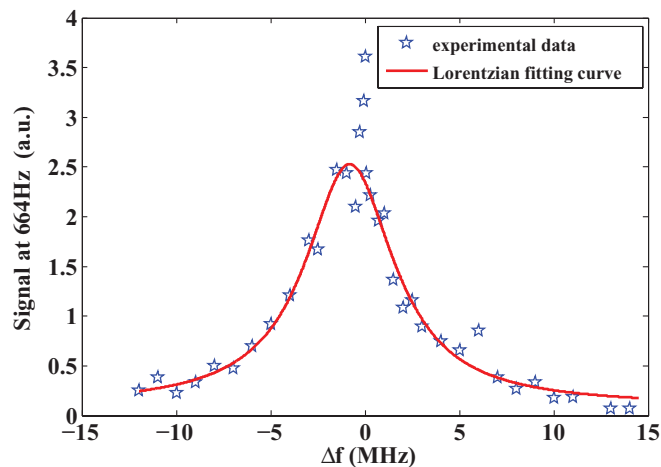


FIG. 5. (Color online) Ce ion homogeneous linewidth measured using saturation spectroscopy. The pentagrams are the measured data points. The solid curve is a Lorentzian fitting of the points excluding the central four which we believe are affected by population trapping.

by adjusting the spatial overlap between the pump and probe beam. While in principle we have no reason to suspect this, the fact that the center of the Lorentzian fitting curve is not at zero detuning but shifted to the left would indicate this as a possible explanation.

Based on the coherence time (lifetime limited value) and the frequency integrated absorption cross section (in  $\text{m}^2 \text{ rad/s}$ ) calculated from the inhomogeneous line,<sup>21</sup> the absorption cross section of the Ce ion in site 1 and the corresponding saturation intensity were calculated to be  $\sim 4.5(\pm 1.3) \times 10^{-19} \text{ m}^2$  and  $\sim 1.4(\pm 0.4) \times 10^7 \text{ W/m}^2$ , respectively.

The experimental data indicate an increased interaction between the beams within a narrow range ( $\sim 400 \text{ kHz}$ ) of frequency detuning close to the line center. The origin of this resonance was not investigated but narrow resonances of this type can occur if the upper state can also decay to a third level which (compared with the relaxation from the excited state) relaxes slowly to the ground state; see, e.g., Refs. 22 and 23. The linewidth of the resonance is then determined by the decay rate of this third level. In the present experiment the third level could possibly be one of the lowest Kramer's doublets on the  $^2F_{5/2}$  ( $4f$ ) ground state, compared with, e.g., Ref. 24, and the intrinsic width of the narrow resonance would then be given by the spin-lattice relaxation rate of the ground state. Using the calculated saturation intensity, the signal at the sum frequency (664 Hz) should be about 0.1% of the signal at 362 Hz at zero detuning frequency. However, the actual sum frequency signal is a factor of 8 higher than expected. The existence of a third level may not only give rise to the narrow structure mentioned above but also could provide a larger saturation effect due to the trapping of ions in this level. This could be part of the reason why the signal at 664 Hz (0.8% of the signal at 362 Hz) is larger than expected.

### C. Ce-Pr interaction

The Ce and Pr ions in  $\text{Y}_2\text{SiO}_5$  have different permanent electric dipole moments in their ground and excited states as they sit in noncentrosymmetric sites. This difference in the

ground- and excited-state permanent dipole moment is denoted as  $\Delta\mu$ . When one ion is changing its state from ground to excited state or vice versa, the surrounding electric field is changed. This permanent dipole-dipole interaction causes a frequency shift  $\Delta f$  of the transition lines of the nearby ions, which depends on the spatial distance  $r$  between those two ions and  $\Delta\mu$  of both ions as<sup>25</sup>

$$\Delta f \propto \frac{\Delta\mu_{\text{Ce}}\Delta\mu_{\text{Pr}}}{r^3} \kappa(\Delta\hat{\mu}_{\text{Pr}}, \Delta\hat{\mu}_{\text{Ce}}, \hat{r}), \quad (1)$$

where

$$\kappa(\Delta\hat{\mu}_{\text{Pr}}, \Delta\hat{\mu}_{\text{Ce}}, \hat{r}) = \Delta\hat{\mu}_{\text{Ce}} \cdot \Delta\hat{\mu}_{\text{Pr}} - 3(\hat{r} \cdot \Delta\hat{\mu}_{\text{Ce}})(\hat{r} \cdot \Delta\hat{\mu}_{\text{Pr}}) \quad (2)$$

stands for dependence of the interaction on the dipole orientations and displacement.  $\Delta\hat{\mu}_{\text{Pr,Ce}}$  and  $\hat{r}$  are the unit vectors of the permanent dipole moment change and the displacement between these two dipoles (in our case they are a Pr dipole and a Ce dipole). Since the shift arises from the permanent dipole moment changes and not the transition dipole interactions, the shifts are the same regardless of which ion is excited for two ions with a specific distance. The value of  $\Delta\mu_{\text{Ce}}$  of the  $\text{Ce}^{3+} 4f-5d$  transition in  $\text{Y}_2\text{SiO}_5$  is not previously known. It can, e.g., be determined by measuring the Stark shift caused by the interaction between the ions and an external electric field.<sup>26</sup> Here we instead used a sample doped with both  $\text{Ce}^{3+}$  and  $\text{Pr}^{3+}$  and implemented a two-pulse photon echo experiment on Pr ions, where Ce ions were excited during the dephasing period of the Pr ions, and the reduction of the echo intensity was observed.<sup>25</sup> The reduction is caused by the fact that a subgroup of Pr ions experience a frequency shift induced by the excitation of nearby Ce ions. When this happens the phases of the Pr superposition states evolve at different rates in the dephasing and rephasing periods, which causes an echo intensity decrease which depends on the magnitude of the shift and the evolution time. Thus the Pr-Ce ion-ion interaction introduces an additional dephasing channel for the excited Pr ions, which broadens the Pr homogeneous linewidth. From this extra broadening  $\Delta\mu_{\text{Ce}}$  can be calculated.<sup>27</sup>

In this experiment, an actively stabilized dye laser with a linewidth of less than 1 kHz was used to excite the  $\text{Pr } ^3H_4 \rightarrow ^1D_2$  transition at 606 nm. Two weak Gaussian pulses with power of  $\sim 0.5 \text{ mW}$  ( $0.15\text{-}\mu\text{s}$  duration time) were created with an AOM and the photon echo from the Pr ions was recorded. Ce ions were excited during the dephasing time of the Pr ions using an external cavity diode laser and another AOM. The pulse sequence is shown in Fig. 6, where eraser pulses refer to several frequency scanning pulses at 606 nm. These were applied to shuffle the Pr ions between the hyperfine states and prevent persistent hole burning that would otherwise be created by the two Gaussian pulses (pulse 1 and pulse 2) over

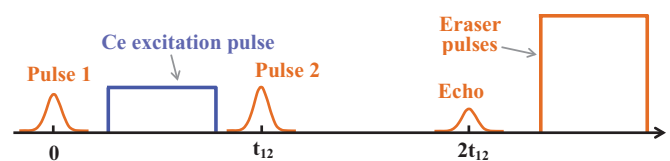


FIG. 6. (Color online) Pulses sequence for the Ce-Pr interaction measurement.

time. Each laser beam was coupled into a single mode fiber for spatial mode cleaning, and the collimated output beams from the fibers were coupled together by a dichroic mirror with 90% transmission (reflection) for 606 nm (371 nm). Those two beams were focused onto the crystal with focal diameters of about 130 and 170  $\mu\text{m}$ , respectively, by a low dispersion  $\text{CaF}_2$  lens. The spatial mode overlap between the two beams within the crystal was ascertained by using a beam profiler to ensure that the center of the two beam profiles overlapped with each other within 10  $\mu\text{m}$  over the 40-cm distance between the dichroic mirror and the common focusing lens. The echo signal was deflected by a third AOM into a photomultiplier tube (PMT). Right before the PMT an electronic shutter with 100- $\mu\text{s}$  rise time was used to prevent the strong frequency scanning pulses from reaching the PMT after the echo was recorded.

The intensity of the echo from the Pr ions was recorded as a function of the separation time  $t_{12}$  in two situations: Ce ions being excited or not excited (Ce laser blocked) in between the two Pr excitation pulses. The excitation of Ce ions was implemented at wavelengths of either 370.83 nm (hereafter referred to as online) or 371.54 nm (referred to as offline). Here online (offline) refers to the fact that the excitation wavelength is on (off) the ZPL of Ce ions in site 1. It is worthwhile to note that even at the offline wavelength there is still considerable background absorption as can be seen in the absorption spectrum in Fig. 3. We believe that this comes from ions in site 2, and they will also cause a reduction of the photon echo from Pr ions, by the interaction shown in Eq. (1). The experimental data from a Pr:Ce:Y<sub>2</sub>SiO<sub>5</sub> crystal (grown by Shanghai Institute of Ceramics in China) with 0.05% of Pr and 0.088% of Ce dopant concentration relative to the Y ions are shown in Fig. 7.

Four series of data were recorded. The circles are the echo signals from the Pr ions when Ce ions were excited online (excitation power  $\sim 0.5$  mW) during the dephasing time  $t_{12}$ . Each point is an average value of  $\sim 30$  shots, and the error

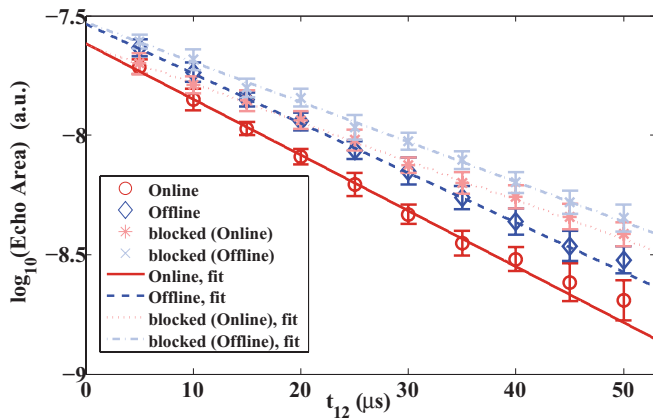


FIG. 7. (Color online) Decay curve of the echo from the Pr ions on the Pr:Ce:Y<sub>2</sub>SiO<sub>5</sub> crystal. The circles (diamonds) are the experimental echo signal when the Ce ions were excited at an online (offline) wavelength. Error bar shows the standard deviation. The solid, dashed lines are logarithmic fits corresponding to those two cases. The stars (crosses) are the experimental data when the Ce excitation laser was blocked. The difference between them is explained in the text.

TABLE I. Measured homogeneous linewidths of Pr ions  $^3H_4 \rightarrow ^1D_2$  transition with Ce excitation laser being at an online wavelength, offline wavelength, and turned off.

Measured values (Pr)	Ce online		Ce offline	
	Laser on	Laser off	Laser on	Laser off
$T_2$ ( $\mu\text{s}$ )	$74 \pm 2$	$107 \pm 3$	$83 \pm 1$	$104 \pm 3$
$\Gamma_{\text{hom}}$ (kHz)	$4.3 \pm 0.1$	$3.0 \pm 0.1$	$3.83 \pm 0.05$	$3.1 \pm 0.1$

bar shows the standard deviation. To verify the experimental data, a complimentary data point corresponding to each circle, shown as a star, was recorded as well with the Ce excitation laser blocked. At each value of  $t_{12}$  in Fig. 7, all shots of the circle point were recorded first followed by the shots of the corresponding star point. After recording all data points at various  $t_{12}$ , the Ce laser was tuned to the offline position. The corresponding set of data was recorded, shown by the diamonds (Ce laser offline) and crosses (Ce laser blocked). The solid, dotted, dashed, and dash-dotted lines are the logarithmic fits of the experimental data for the cases when the Ce laser is online, blocked, offline, and blocked, respectively. The two blocked cases are equivalent, but show an offset on the echo signal possibly caused by laser power drift. However, the slopes are the same within the margin of error, as expected. The echo intensity as a function of the pulse separation time is

$$I_{\text{echo}} = I_0 e^{-4t_{12}/T_2}, \quad (3)$$

where  $I_0$  is the maximum echo intensity when extrapolating the separation time to zero. Results of the measurements are shown in Table I, where  $T_2$  and  $\Gamma_{\text{hom}}$  refer to the coherence time (with 70% confidence interval) and homogeneous linewidth of the Pr ions transition, respectively.

Table I shows that the homogeneous linewidth broadening caused by the Ce online excitation  $\Gamma_{br}$  is 1.3 kHz with  $\pm 0.14$  kHz for a 70% confidence interval, while for the Ce offline excitation the broadening is  $\sim 0.7$  kHz ( $\pm 0.11$  kHz). The difference between these two values tells the broadening contribution only from the Ce ions in site 1, which is  $\sim 0.6$  ( $\pm 0.18$ ) kHz. This value was used for calculating  $\Delta\mu_{\text{Ce}}$  in the following passage.

However, the reduction in echo intensity could conceivably be caused by other reasons than a frequency shift resulting from the permanent dipole-dipole interaction. For instance, (1) the Pr ions directly absorb the ultraviolet (UV) photons leading to processes shortening the coherence time, which causes the echo intensity to decrease, although this is unlikely to happen, as seen from the literature.<sup>28</sup> (2) The energy is transferred from Ce ions to Pr ions so that Pr ions are excited to a higher level, which also can cause an echo reduction. To clarify the influence of suggestion (1) above we did exactly the same measurement as before but on an Y<sub>2</sub>SiO<sub>5</sub> crystal with the same Pr dopant concentration but no Ce ions. The result is shown in Fig. 8, where the Pr homogeneous linewidths are the same when the laser pulse at the Ce absorption wavelength was present and absent, which means that the linewidth broadening shown in Fig. 7 does not result from direct UV absorption by the Pr ions. For clarifying whether the interaction can be induced by energy transfer [argument (2) above], we did an

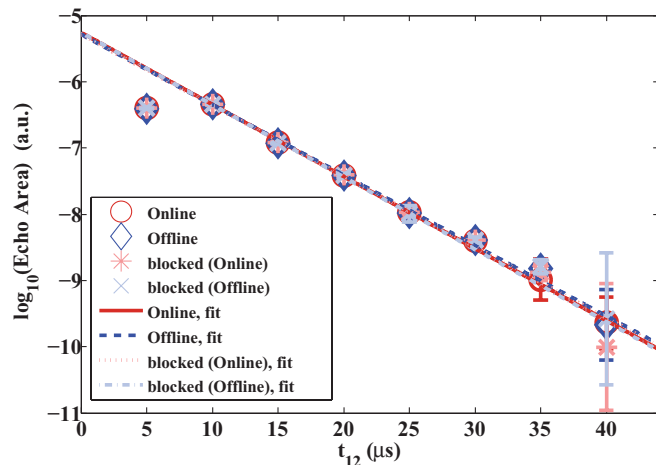


FIG. 8. (Color online) Echo decay curve on the pure Pr:Y<sub>2</sub>SiO<sub>5</sub> crystal. Notation of the data symbols is the same as in Fig. 7. Circles, diamonds, stars, and crosses are for the cases when the Ce laser is online, offline, blocked (online), and blocked (offline), respectively. Deviation of the first data point from the fitting line was caused by the saturation of the PMT.

excited-state population decay measurement on Pr ions in the Pr:Ce:Y<sub>2</sub>SiO<sub>5</sub> crystal as follows: (i) A zero absorption spectral window centered at frequency  $\nu_0$  was created using optical pumping.<sup>29</sup> (ii) A subset of Pr ions having their transition at frequency  $\nu_0$  is transferred to the  $|\pm 5/2g\rangle$  state [the Pr ion level structure is shown in Fig. 2(b)]. (iii) A pulse with area of  $\pi$  excites these ions to their  $|\pm 5/2e\rangle$  state with an efficiency of more than 85%. (iv) A Ce excitation pulse with duration time  $T$  was incident on the crystal. If there is Ce-Pr energy transfer or state changing interactions other than the frequency shifts due to the permanent dipole-dipole interaction, the Pr excited-state population should change. (v) After the time  $T$  the transmission of a pulse scanned in frequency around frequency  $\nu_0$  [see Fig. 2(b)] determines the population difference between the  $|\pm 5/2g\rangle$  and  $|\pm 5/2e\rangle$  state by measuring the absorption (this pulse is called the readout pulse in the following passage). Following the procedure above the Pr population difference (normalized to the initial population in  $|\pm 5/2g\rangle$  state) between the excited and ground state,  $N_e - N_g$ , was recorded as a function of the separation time  $T$  between the  $\pi$  pulse and the readout pulse for the two cases where Ce ions were excited or not excited during the time  $T$ .

Figure 9 shows that the population differences of Pr ions when Ce ions are excited (online) and not excited (blocked) agree with each other within 3%. Similar measurements from the Ce offline excitation and Ce laser blocked cases also show the same result. Thus no effect of energy transfer between the Ce and Pr ions was observed. Based on the test on the pure Pr doped crystal (Fig. 8) and this excited-state population decay measurement of Pr ion (Fig. 9), to the best of our knowledge, the homogeneous broadening shown in Fig. 7 should be caused by the permanent dipole-dipole interaction between the Pr and Ce ions.

The homogeneous linewidth broadening induced by the permanent dipole-dipole interaction  $\Gamma_{br}$  relates to the  $\Delta\mu$  of

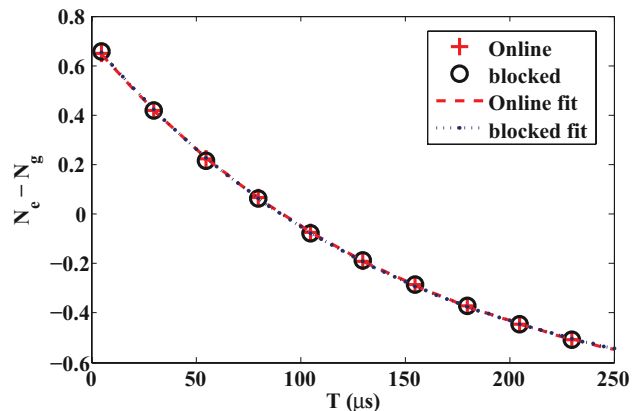


FIG. 9. (Color online) Population difference between the excited and ground state of Pr ions in a Pr:Ce:Y<sub>2</sub>SiO<sub>5</sub> crystal as a function of time with Ce online excitation (+) and Ce laser blocked (○). The dashed and dot-dashed lines are the respective exponential curve fittings. The standard deviation of the data points is  $\sim 2\%$ .

the interacting ions as<sup>27</sup>

$$\Gamma_{br} = \frac{1}{2\pi} C D_0 \langle W_{Ce} \rangle, \quad (4)$$

where

$$C = \frac{2}{3} \pi^2 p \langle |\kappa| \rangle, \quad (5)$$

$p$  represents the occupation probability of the Ce ions relative to the total number of ions in the crystal, and  $\langle |\kappa| \rangle$  is in the order of 1,<sup>25</sup> representing the averaged value of  $\kappa$  [shown in Eq. (2)] over all angles defining the relative dipole orientations and the orientations between dipoles and the displacement.

$D_0$  describes the magnitude of the permanent dipole-dipole interaction with a unit distance of  $r_0$ ,

$$D_0 = \eta(0) \frac{\Delta\mu_{Ce} \Delta\mu_{Pr}}{4\pi \epsilon_0 \hbar r_0^3}, \quad (6)$$

where  $\Delta\mu_{Ce}$  and  $\Delta\mu_{Pr}$  is the difference of the permanent dipole moment in the ground and excited state of Ce and Pr ions, respectively.  $\eta(0) = 1.28$  represents the dielectric correction factor for long-range dipole-dipole interaction.<sup>30</sup>  $\epsilon_0$  is the vacuum permittivity.  $r_0$  stands for the length of the cube which one ion occupies on average.  $\langle W_{Ce} \rangle$  represents the average excitation probability of the Ce ions contributing to the interaction during the dephasing time.

For the crystal used in this experiment, the occupation probability  $p \simeq 1.92 \times 10^{-4}$  considering a 87% occupation on site 1.<sup>31</sup>  $\langle W_{Ce} \rangle \simeq 1.8(\pm 0.7) \times 10^{-7}$ , which is estimated from the saturation intensity (shown in Sec. II B) and integrated over the inhomogeneous line as in Ref. 27. The excitation intensity used for the estimation is the average value over a volume with the beam diameter of  $\rho_{fwhm}$ , the full width at half maximum of the Pr excitation laser intensity, through the crystal thickness of 1 mm.  $\Delta\mu_{Ce}$  (site 1) is calculated as  $9.6(\pm 5.3) \times 10^{-30}$  C m using Eqs. (3)–(5) with  $r_0 = 0.237$  nm,  $\langle |\kappa| \rangle_{\Omega} \simeq 0.7$ , and  $\Delta\mu_{Pr} = 2.43 \times 10^{-31}$  C m.<sup>27</sup> We also calculated  $\langle W_{Ce} \rangle$  from the ratio of the number of absorbed photons (equivalently number of excited Ce ions) during 40 ns over the total number of Ce ions in site 1 for a certain volume (given by the laser

beam profile). The value is  $1.8(\pm 0.4) \times 10^{-7}$ , which agrees with the previous value very well.

The measured value of  $\Delta\mu_{\text{Ce}}$  (site 1) is an encouraging result as it indicates that the transition line of a Ce ion will be shifted by more than 300 MHz on average due to the change of states of a nearby Pr ion in a Pr:Ce:Y<sub>2</sub>SiO<sub>5</sub> crystal with a dopant concentration of 0.05% (the average ion-ion distance is  $\sim 5$  nm). This shift is clearly large enough to force the Ce ions in site 1 out of resonance with the readout laser which is initially on resonance. However, this shift does not prohibit the excitation of the Ce ions in site 2 since these ions are not excited at their zero-phonon line and the absorption spectrum is much broader than the permanent dipole-dipole interaction induced shift. This gives us a background fluorescence even if the single Ce ion in site 1 is shifted out of resonance. However, based on our preliminary investigation the fluorescence contrast within the range 380–420 nm (as shown in Fig. 4) is believed to be good enough for detecting a single Ce ion in site 1 with a reasonable signal-to-noise ratio. So the fluorescence emitted from the Ce ions in site 1 can still be used as an indicator to show which state ( $|0\rangle$  or  $|1\rangle$ ) the Pr ion occupies.

### III. CONCLUSION

The spectroscopic properties of Ce<sup>3+</sup> doped in an Y<sub>2</sub>SiO<sub>5</sub> crystal were characterized for investigating the possibility to use it as a probe for detecting which hyperfine ground state a nearby ion (e.g., Pr) is occupying. Particularly (i) the ZPL of the  $4f$ - $5d$  transition of Ce<sup>3+</sup> doped in Y<sub>2</sub>SiO<sub>5</sub> was found around 370.83 nm with a linewidth of about 50 GHz. (ii) The homogeneous linewidth was measured by intensity modulated saturation spectroscopy to be  $\sim 3$  MHz. It is essentially limited by the excited-state lifetime of that transition, which is the optimal case for using Ce<sup>3+</sup> as a readout ion. In this experiment we also have not observed any signs that there is a long-lived trapping state for Ce ions, which means that the fluorescence can be cycled as many times as needed. From the linewidth measurements the oscillator strength, absorption cross section, and saturation intensity were

calculated to be  $\sim 6.2(\pm 1.7) \times 10^{-7}$ ,  $\sim 4.5(\pm 1.3) \times 10^{-19}$  m<sup>2</sup>, and  $\sim 1.4(\pm 0.4) \times 10^7$  W/m<sup>2</sup>, respectively. (iii) The Ce-Pr interaction was demonstrated through a photon echo experiment and the difference in the permanent dipole moment ( $\Delta\mu_{\text{Ce}}$ , averaged value of all dipole orientations) for the  $4f$  ( $^2F_{5/2}$ ) and lowest  $5d$  states was measured to be  $\sim 9.6(\pm 5.3) \times 10^{-30}$  C m, which is sufficiently large to provide a frequency shift much larger than the Ce homogeneous linewidth for a suitable dopant concentration of qubit ions. The data obtained so far shows that the Ce ion is a very promising readout ion candidate and a setup for single Ce ion detection by observing the  $5d$ - $4f$  fluorescence is currently under construction. Single Ce ion detection in a YAG (Y<sub>2</sub>Al<sub>5</sub>O<sub>12</sub>) crystal was recently demonstrated.<sup>32</sup> The ability of state selective readout of a single rare-earth ion in inorganic crystals would be a significant step forward for quantum computing in these materials where high fidelity gate operations on ensembles have already been carried out.<sup>7,8</sup> It also opens the possibility to use rare-earth ions as extraordinarily sensitive probes of the local environment in these types of crystals. The ability to carry out (and read out) operations on individual ions would strongly address the scalability problem and greatly reduce the qubit operation time since fewer and simpler pulses can be used when the dephasing caused by the inhomogeneous broadening is no longer a concern. It is also quite clear that rare-earth ion doped crystals generally have excellent properties for preserving quantum states seen from the impressive quantum memory development that is taking place in these materials.<sup>33–35</sup>

### ACKNOWLEDGMENTS

We thank M. Bettinelli for the helpful discussion. This work was supported by the Swedish Research Council (VR), the Knut and Alice Wallenberg Foundation (KAW), the Maja och Erik Lindqvists forskningsstiftelse, the Crafoord Foundation and the EC FP7 Contract No. 247743 (QuRep), (Marie Curie Action) REA Grant Agreement No. 287252 (CIPRIS), Lund Laser Center (LLC), and the Nanometer Structure Consortium at Lund University (nmC@LU).

\*Corresponding author: yan.ying@fyisk.lth.se

<sup>1</sup>T. D. Ladd, F. Jelezko, R. Laflamme, Y. Nakamura, C. Monroe, and J. L. O'Brien, *Nature (London)* **464**, 08812 (2010).

<sup>2</sup>R. Blatt and D. Wineland, *Nature (London)* **453**, 1008 (2008).

<sup>3</sup>J. A. Jones, *Prog. NMR Spectrosc.* **59**, 91 (2011).

<sup>4</sup>J. H. Plantenberg, P. C. de Groot, C. J. P. M. Harmans, and J. E. Mooij, *Nature (London)* **447**, 836 (2007).

<sup>5</sup>A. P. Nizovtsev, S. Ya. Kilin, F. Jelezko, T. Gaebel, I. Popa, A. Gruber, and J. Wrachtrup, *Opt. Spectrosc.* **99**, 233 (2005).

<sup>6</sup>N. Ohlsson, R. K. Mohan, and S. Kröll, *Opt. Commun.* **201**, 71 (2002).

<sup>7</sup>J. J. Longdell and M. J. Sellars, *Phys. Rev. A* **69**, 032307 (2004).

<sup>8</sup>L. Rippe, B. Julsgaard, A. Walther, Y. Ying, and S. Kröll, *Phys. Rev. A* **77**, 022307 (2008).

<sup>9</sup>L. Rippe, M. Nilsson, S. Kröll, R. Klieber, and D. Suter, *Phys. Rev. A* **71**, 062328 (2005).

<sup>10</sup>J. H. Wesenberg, K. Mølmer, L. Rippe, and S. Kröll, *Phys. Rev. A* **75**, 012304 (2007).

<sup>11</sup>S. Bengtsson, Master thesis, Lund University, Sweden, 2012.

<sup>12</sup>A. Walther, B. Julsgaard, L. Rippe, Y. Ying, S. Kröll, R. Fisher, and S. Glaser, *Phys. Scr.* **T137**, 014009 (2009).

<sup>13</sup>Suggested by Olivier Guillot-Noël in the European Quantum Information Processing and Computing workshop, Rome, 2004.

<sup>14</sup>H. Suzuki, T. A. Tombrello, C. L. Melcher, and J. S. Schweitzer, *Nucl. Instrum. Methods Phys. Res. A* **320**, 263 (1992).

<sup>15</sup>T. Aitasalo, J. Hlisa, M. Lastusaari, J. Legendziewicz, J. Niittykoski, and F. Pell, *Opt. Mater.* **26**, 107 (2004).

<sup>16</sup>J. E. Hernandez, Master thesis, Lund University, Sweden, 2006.

<sup>17</sup>B. Henderson and G. F. Imbusch, *Optical Spectroscopy of Inorganic Solids* (Oxford University Press, New York, 1989), p. 262, Eq. (6.10a).

<sup>18</sup>A. Smakula, *Z. Phys.* **59**, 603 (1930).

<sup>19</sup>W. Drozdowski, A. J. Wojtowicz, D. Wisniewski, P. Szupryczynski, S. Janus, J. Lefaucheur, and Z. Gou, *J. Alloy. Compd.* **380**, 146 (2004).

<sup>20</sup>S. Völker, *Annu. Rev. Phys. Chem.* **40**, 499 (1989).

- <sup>21</sup>R. C. Hilborn, *Am. J. Phys.* **50**, 982 (1982).
- <sup>22</sup>D. G. Steel and S. C. Rand, *Phys. Rev. Lett.* **55**, 2285 (1985).
- <sup>23</sup>M. Mitsunaga, N. Uesugi, and K. Sugiyama, *Opt. Lett.* **18**, 1256 (1993).
- <sup>24</sup>R. Kolesov, *Phys. Rev. A* **76**, 043831 (2007).
- <sup>25</sup>S. B. Altner, G. Zumofen, U. P. Wild, and M. Mitsunaga, *Phys. Rev. B* **54**, 17493 (1996).
- <sup>26</sup>F. R. Graf, A. Renn, U. P. Wild, and M. Mitsunaga, *Phys. Rev. B* **55**, 11225 (1997).
- <sup>27</sup>F. R. Graf, A. Renn, G. Zumofen, and U. P. Wild, *Phys. Rev. B* **58**, 5462 (1998).
- <sup>28</sup>N. V. Kuleshov, V. G. Shcherbitsky, A. A. Lagatskya, V. P. Mikhailov, B. I. Minkov, T. Danger, T. Sandrock, and G. Huber, *J. Lumin.* **71**, 27 (1997).
- <sup>29</sup>M. Nilsson, L. Rippe, S. Kröll, R. Klieber, and D. Suter, *Phys. Rev. B* **70**, 214116 (2004).
- <sup>30</sup>G. D. Mahan, *Phys. Rev.* **153**, 983 (1967).
- <sup>31</sup>Y. C. Sun, in *Spectroscopic Properties of Rare Earths in Optical Materials*, edited by G. Liu and B. Jacquier (Springer, Berlin, 2005), Chap. 7.
- <sup>32</sup>R. Kolesov, K. Xia, R. Reuter, R. Stöhr, T. Inal, P. Siyushev, and J. Wrachtrup, *arXiv:1301.5215*.
- <sup>33</sup>M. P. Hedges, J. J. Longdell, Y. M. Li, and M. J. Sellars, *Nature (London)* **465**, 1052 (2010).
- <sup>34</sup>E. Saglamyurek, N. Sinclair, J. Jin, J. A. Slater, D. Oblak, F. Bussières, M. George, R. Ricken, W. Sohler, and W. Tittel, *Nature (London)* **469**, 512 (2011).
- <sup>35</sup>I. Usmani, Ch. Clasusen, F. Bussières, N. Sangouard, M. Afzelius, and N. Gisin, *Nat. Photon.* **6**, 234 (2012).